Predictability of Tropical Cyclone Intensity over the Western North Pacific Using the IBTrACS Dataset

QUANJIA ZHONG

State Key Laboratory of Numerical Modeling for Atmospheric Sciences and Geophysical Fluid Dynamics (LASG), Institute of Atmospheric Physics, Chinese Academy of Sciences, Beijing, and Laboratory for Regional Oceanography and Numerical Modeling, Qingdao National Laboratory for Marine Science and Technology, Qingdao, and College of Earth Science, University of Chinese Academy of Sciences, Beijing, China

JIANPING LI

Laboratory for Regional Oceanography and Numerical Modeling, Qingdao National Laboratory for Marine Science and Technology, Qingdao, and College of Global Change and Earth System Sciences, Beijing Normal University, Beijing, China

LIFENG ZHANG

College of Meteorology and Oceanography, National University of Defense Technology, Nanjing, China

RUIQIANG DING

State Key Laboratory of Numerical Modeling for Atmospheric Sciences and Geophysical Fluid Dynamics (LASG), Institute of Atmospheric Physics, Chinese Academy of Sciences, Beijing, and Laboratory for Regional Oceanography and Numerical Modeling, Qingdao National Laboratory for Marine Science and Technology, Qingdao, China

BAOSHENG LI

State Key Laboratory of Numerical Modeling for Atmospheric Sciences and Geophysical Fluid Dynamics (LASG), Institute of Atmospheric Physics, Chinese Academy of Sciences, Beijing, China

(Manuscript received 18 October 2017, in final form 9 June 2018)

ABSTRACT

The predictability limits of tropical cyclone (TC) intensity over the western North Pacific (WNP) are investigated using TC best track data. The results show that the predictability limit of the TC minimum central pressure (MCP) is ~102 h, comparable to that of the TC maximum sustained wind (MSW). The spatial distribution of the predictability limit of the TC MCP over the WNP is similar to that of the TC MSW, and both gradually decrease from the eastern WNP (EWNP) to the South China Sea (SCS). The predictability limits of the TC MCP and MSW are relatively high over the southeastern WNP where the modified accumulated cyclone energy (MACE) is relatively large, whereas they are relatively low over the SCS where the MACE is relatively small. The spatial patterns of the TC lifetime and the lifetime maximum intensity (LMI) are similar to that of the TC MACE. Strong and long-lived TCs, which have relatively long predictability, mainly form in the southwestern WNP. In contrast, weak and short-lived TCs, which have relatively short predictability, mainly form in the SCS. In addition to the dependence of the predictability limit on genesis location, the predictability limits of TC intensity also evolve in the TC life cycle. The predictability limit of the TC MCP (MSW) gradually decreases from 102 (108) h at genesis time (00 h) to 54 (84) h 4 days after TC genesis.

1. Introduction

The accuracy of tropical cyclone (TC) track and intensity forecasts is of particular importance for warning the public to protect life and property in the affected area. The accuracy of TC track forecasts has steadily improved in recent decades along with a global reduction in forecast error for operational hurricane forecast models (Elsberry et al. 2007; DeMaria et al. 2014). However, although many operational and research

Corresponding author: Dr. Ruiqiang Ding, drq@mail.iap.ac.cn

DOI: 10.1175/MWR-D-17-0301.1

centers have made efforts to improve TC intensity forecasts (Gopalakrishnan et al. 2011; Zhang and Weng 2015; Ruf et al. 2016; Weng and Zhang 2016), the TC intensity errors have decreased at a smaller rate than the track errors over the same period. Particularly, the TC intensity forecast skill at shorter lead times (24–48 h) has shown relatively little improvement (DeMaria et al. 2014).

There may be several reasons for this. As reported by Landsea and Franklin (2013), the forecast error of TC intensity at 24 h is comparable to the limit of currently observational uncertainty of TC intensity. In addition, accurate TC track forecasts are not as heavily dependent on model physics and model resolution. Furthermore, the accuracy of TC intensity forecast may be ultimately limited by the predictability due to the chaotic nature of the atmosphere itself (Lorenz 1963, 1969; Palmer et al. 2014; Tao and Zhang 2015; Judt et al. 2016). To further improve forecasts of TC intensity, it is worth determining quantitatively the limit of predictability of TC intensity (Emanuel and Zhang 2016).

TC intensity is not only affected by the large-scale environment, but also by complex physical processes, making it difficult to assess error growth and intrinsic predictability. Many studies of the predictability of TC intensity have used the Weather Research and Forecasting (WRF) Model (Zhang et al. 2014; Tao and Zhang 2015; Zhu et al. 2016), idealized axisymmetric models (Hakim 2011, 2013; Kieu and Moon 2016), and statistical forecasting models (Kaplan et al. 2015; Emanuel and Zhang 2016). For example, Zhang and Tao (2013) explored the influence of environmental parameters on the predictability of TC intensity through a series of idealized simulations using the WRF Model and indicated that the magnitude of vertical wind shear may have an effect on the accuracy of TC intensity forecasts. Similarly, Tao and Zhang (2014) showed the impacts of uncertainty in the vertical wind shear and the spatial distribution of moist convection on the evolution of TCs and found that these uncertainties decrease the predictability of TC intensity. Brown and Hakim (2013) and Hakim (2013) used idealized simulations of a mature TC in an axisymmetric model to examine the predictability of TC intensity, suggesting that the intrinsic predictability of TC near-surface winds is lost after ~72 h. A recent case study by Judt et al. (2016) indicated that the forecast error of TC surface wind shows rapid growth of small-scale uncertainties, but the mean vortex circulation of the TC is comparatively resistant to upscale error growth. Therefore, the relatively long predictability of the environment and the mean vortex could be exploited for longer-term predictions of TC intensity.

The above modeling studies have provided a better understanding of TC intensity predictability, which is helpful in improving the forecast skill of TC intensity. However, some of the aforementioned studies are limited, as they rely heavily on idealized numerical models with periodic boundary conditions and/or start from identical initial conditions (Judt et al. 2016). While numerical models have been helpful in assessing the influence of the uncertainty of environmental variables on the forecast uncertainty and predictability of TC intensity, almost all numerical models of TCs used in previous studies (Weng and Zhang 2016; Zhu et al. 2016), such as the WRF Model, are imperfect, and model shortcomings hinder the simulation of TC intensity. The estimate of TC intensity predictability is significantly influenced by model error owing to the model deficiencies; consequently, such an estimate cannot truly represent the real predictability of TC intensity. Another challenge is that our understanding of TC intensity predictability is derived mainly from analyses of TC case studies. Although TCs are viewed as highly episodic, isolated events, the characteristics of TCs vary widely with genesis location, and the spatial distribution of the TC intensity predictability limit remains unknown.

The goal of this study is to quantitatively determine the predictability limit of two different measures of TC intensity [the minimum central pressure (MCP) and maximum sustained wind (MSW)] over the whole western North Pacific (WNP) using observational data (observed TC best track data in this study). This work builds on our recent work on the predictability of TC tracks (Zhong et al. 2018, hereafter Z18), where we use best track data to show that the mean predictability limit of all TC tracks over the WNP basin is ~108 h. The observed best track data include a significant amount of position and intensity information for TCs. Therefore, the best track data can be used to determine the predictability limit of TC intensity, as satisfactory models are not available to predict TC intensity.

A method has been proposed to investigate the predictability of chaotic systems using the nonlinear local Lyapunov exponent (NLLE) (Chen et al. 2006; Ding and Li 2007). The NLLE allows the predictability limit of dynamical systems, such as a chaotic system, to be determined quantitatively. For a low-order chaotic system, the leading NLLE mainly describes the average growth rates of the initial error in the fastest-growing direction. Meanwhile, to assess the actual atmospheric

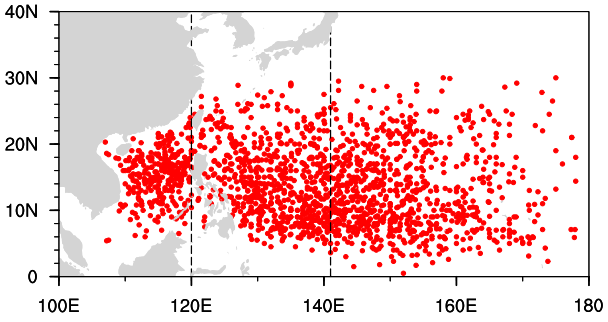

FIG. 1. Spatial distribution of genesis locations of all TCs over the whole WNP basin. The red dots denote the genesis locations of TCs. The lines at 120° and 141°E (the longitude of the mean genesis location of all TCs over the WNP) are the longitudinal boundaries of the three subregions: the SCS, WWNP, and EWNP.

predictability from observational data, a practical and efficient algorithm known as local dynamical analogs (LDAs), has been devised to enable the calculation of the NLLE (Li and Ding 2011). Similarly, the limit of TC intensity predictability in this work can therefore be assessed from the observed best track data using the LDAs algorithm. Here, it should be noted that the predictability limit of TC intensity obtained in this work would be lower than the intrinsic predictability, which may be achieved only if the prediction model is perfect except for sufficiently small error in the initial conditions.

The remainder of the paper is organized as follows. Section 2 describes the observational data and introduces the NLLE approach. The main results regarding the predictability limit of TC intensity and its spatial distribution are presented in section 3. Section 4 provides a summary and discussion.

2. Data and methodology

a. Observational data

Tropical cyclone best track data were obtained from the International Best Track Archive for Climate Stewardship (IBTrACS) dataset, which combines the TC best track data from all forecasting agencies into an integrated dataset (https://www.ncdc.noaa.gov/ibtracs/index.php?name=ibtracs-samples). The IBTrACS dataset consists of the best estimates of the TC central position (latitude and longitude), MCP, and MSW at 6-hourly intervals (Knapp and Kruk 2010; Knapp et al. 2010). The pressure and wind speed of the TC represent two metrics of TC intensity, so the predictability limits of the TC MCP and MSW are investigated separately using the best track data. We use TC best track data for the period 1945–2015, and the WNP basin is defined as the region 0°–30°N, 100°E–180° including the South China Sea (SCS).

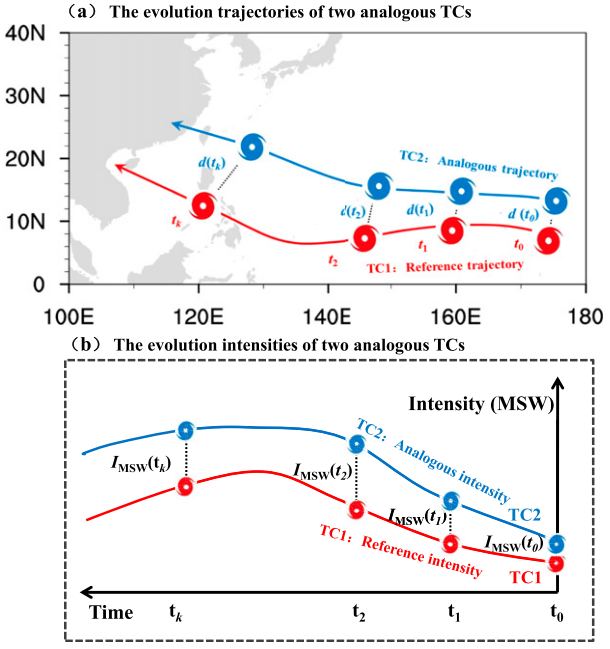

FIG. 2. Schematic representation of the procedure used to calculate the NLLE from the best track data. (a) The trajectory of an analog of the reference TC at time t_i ($i = 0, 1, 2, \ldots, k$) is denoted as an analogous trajectory. (b) Evolution of the intensity of an analog of the reference TC at time t_i ($i = 0, 1, 2, \ldots, k$) is denoted as an analogous intensity. The growth rate of the absolute distance error (absolute intensity error) between the reference trajectory (intensity) and its analogous trajectory (intensity) is used to estimate the NLLE.

b. The NLLE approach

The NLLE approach can be used for quantitative estimation of the predictability limit of atmospheric and oceanic variables. For a variable $\mathbf{x}(t_0)$ at time t_0, the NLLE λ is defined as follows:

$$\lambda[\mathbf{x}(t_0), \boldsymbol{\delta}(t_0), \tau] = \frac{1}{\tau} \ln \frac{\|\boldsymbol{\delta}(t_0 + \tau)\|}{\|\boldsymbol{\delta}(t_0)\|}, \quad (1)$$

where $\lambda[\mathbf{x}(t_0), \boldsymbol{\delta}(t_0), \tau]$ depends on the initial state $\mathbf{x}(t_0)$ of the reference orbit in phase space, the initial error $\boldsymbol{\delta}(t_0)$, and the evolution time τ (Chen et al. 2006; Ding et al. 2007; Ding and Li 2007). The NLLE λ mainly describes the growth rates of the initial error of the dynamic system. Based on the NLLE, the mean relative growth of the initial error (RGIE), which is defined as the ratio of the error at the evolution time τ to the initial error, can be obtained from

$$\overline{\Phi}[\boldsymbol{\delta}(t_0), \tau] = \exp\{\overline{\lambda}[\boldsymbol{\delta}(t_0), \tau]\tau\} \xrightarrow{P} c(N \to \infty), \quad (2)$$

where $\xrightarrow{P}$ denotes the convergence in probability, and $\overline{\lambda}[\boldsymbol{\delta}(t_0), \tau]$ is the ensemble mean NLLE of the dynamic

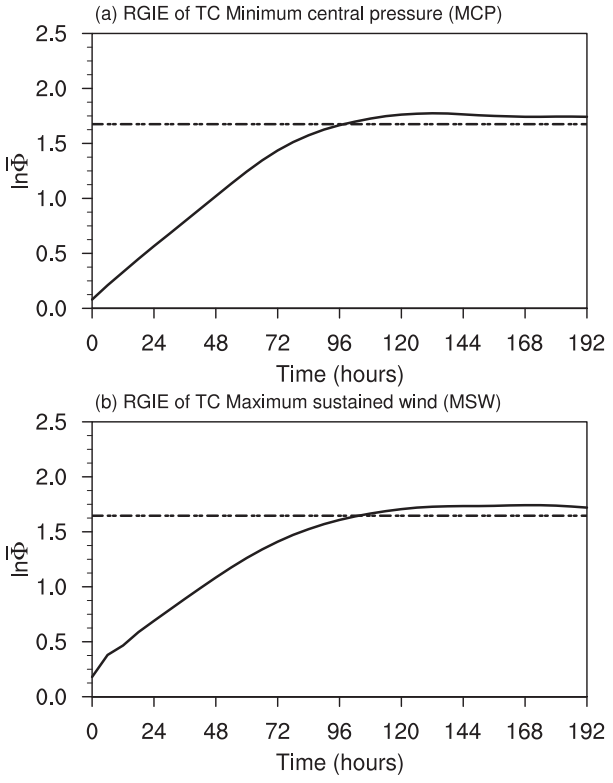

FIG. 3. The logarithm of mean error growth of all TC (a) minimum central pressure (MCP) and (b) maximum sustained wind (MSW) over the whole WNP basin, as obtained from the IBTrACS best track data. Note that the mean error growth as a function of the time is calculated only for the TC at the genesis time, but not for each time of TC life cycle. The dashed line represents the 95% level of the saturation value, as obtained by taking the average of the mean error growth after 144 h.

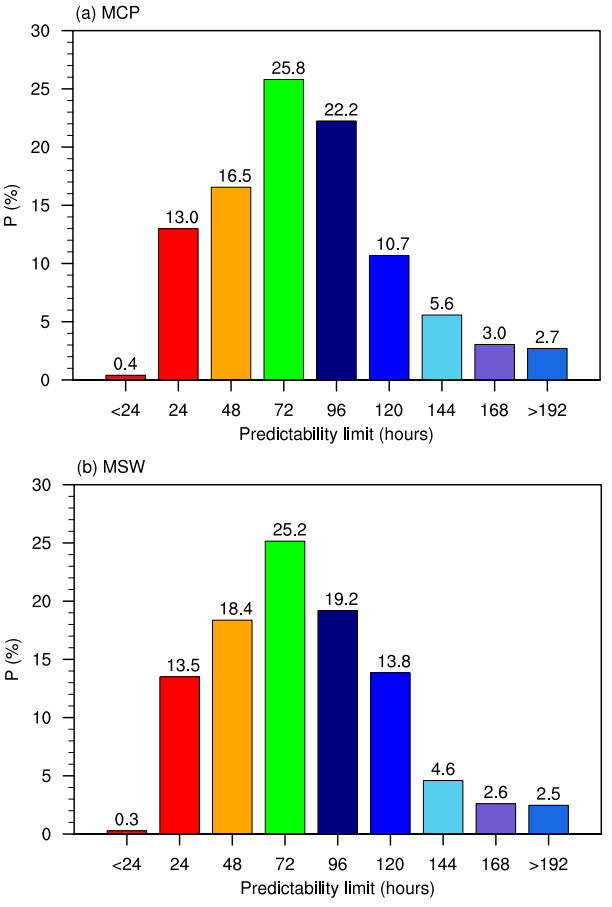

FIG. 4. Probability (%) distribution of the predictability limit of the TC (a) minimum central pressure (MCP) and (b) maximum sustained wind (MSW) as calculated only for the TC at genesis time.

system. Using the theorem from Ding and Li (2007), the constant c can be considered as the theoretical saturation level of the RGIE, when the sample size N tends to infinity. When the mean error reaches the saturation level, the initial information is lost and predicting the state variables of the system becomes meaningless. Therefore, the predictability limit can be quantitatively determined based on the theoretical saturation value (Ding and Li 2007), meaning that an accurate prediction of the system's state variables cannot be made, once the forecast lead time is beyond this upper limit of time.

If the equations governing dynamic systems are known, the mean NLLE can be directly obtained from the error evolution equations of the systems. However, the error evolution equations are not known explicitly for the real atmosphere, because of imprecisely known parameters and external forcing terms (Ding and Li 2007). In this case, the NLLE may be estimated from the atmospheric observational data using the LDAs algorithm (Ding et al. 2010, 2011; Li and Ding 2011; Ding et al. 2016; Liu et al. 2016). In this study, the NLLE method and the LDAs algorithm are applied to find the TC analog(s) that have similar characteristics, such as similar track and intensity, and to estimate the predictability of TC intensity.

c. *Calculation of the NLLE from best track data*

Figure 1 shows the spatial distribution of TC genesis location (defined as the position of the first record of a TC track in the best track data) over the whole WNP basin for the period 1945–2015. More than 2000 TCs formed during this period. For the purpose of the present study we excluded TCs with lifetimes less than 48 h and TCs with observational values of the MCP or MSW missing during the entire period of the TC record. The LDAs algorithm finds the TC analog(s) over the WNP basin using the best track data. Similar to Z18, analogous TCs are two independent TCs with similar location and track length, with small initial distance and

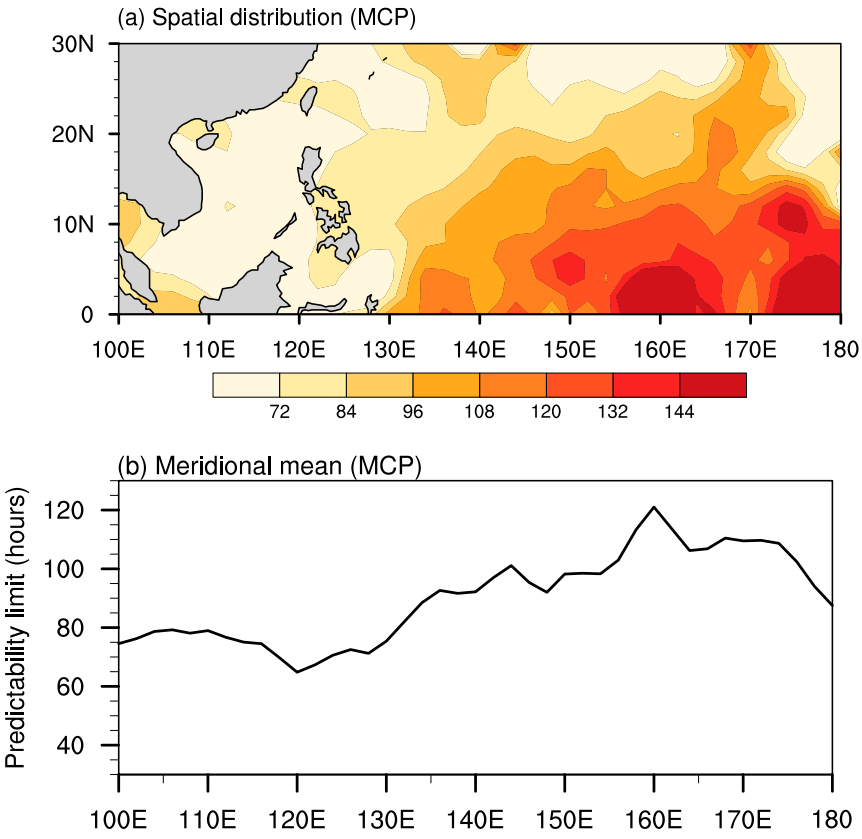

FIG. 5. (a) Spatial distribution of the predictability limit (h) of the individual TC minimum central pressure (MCP) and (b) the meridional mean profile of the predictability limit. Note that the spatial interpolations are based on the TC genesis location.

evolutionary distance between their tracks.[1] Analogous TCs should also have similar initial intensity and evolutionary intensity.[2]

In this study, the initial errors of the TC MCP and MSW are defined as the absolute difference in the MCP and MSW between the analogous TC and its reference TC at the genesis time, while the error at each time point is the absolute difference between the MCP and MSW of the two analogous TCs in their present locations (PLs) (Fig. 2b). The definition of the NLLE means that the error growth rates of the TC MCP and MSW between the reference TC and analog TC can be calculated using the IBTrACS best track data. Because the analogous TCs are based on the similarity of the genesis location and initial intensity, the mean error growth as a function of time is calculated only for the TC at the genesis time but not for each time of TC life cycle. Likewise, the estimate of the predictability limit of TC intensity is only for the TC at the genesis time unless otherwise stated in this paper. A detailed description of the algorithm used to find the analogous TCs and to estimate the NLLE using the best track data is given in appendixes A and B.

3. Results

a. *Predictability limit of TC intensity*

In this study, the mean error growth represents the mean RGIE, which is defined as the ratio of the real-time intensity error at the evolution time to the initial intensity error. Figures 3a and 3b show the log of mean errors in MCP and MSW for all TCs in the WNP, based

[1] The initial distance is a distance (along a great circle) between the locations of the two independent TCs at genesis time, ensuring that the genesis locations of the two independent TCs are close. Similarly, the evolutionary distance is the averaged distance of several present locations between the two independent TCs evolving over an early time interval since TC formed, which is to ensure the similarity of the trajectories of the two independent TCs over a short period of time.

[2] The initial intensity is the first record of the TC intensity, and the evolutionary intensity is the averaged difference in intensity between two different TCs evolving over an early time interval since the TC formed.

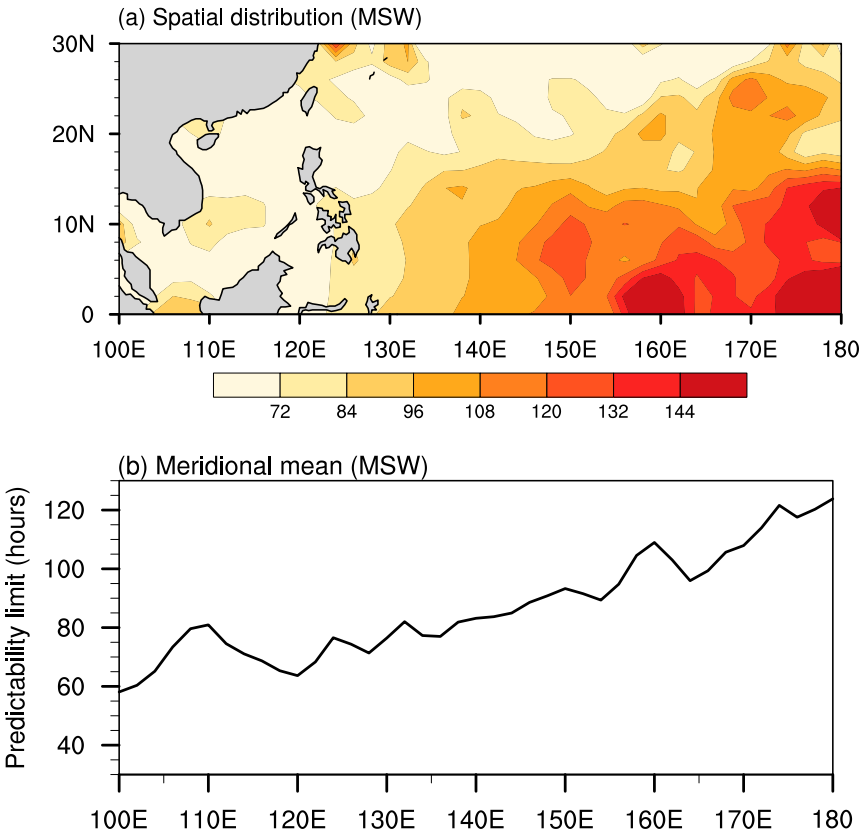

FIG. 6. As in Fig. 5, but for the TC (a) maximum sustained wind (MSW) and (b) its meridional mean profile.

on the IBTrACS dataset. The linear evolution up to 72 h in Fig. 3 indicates that the absolute intensity error growth was exponential, with a growth rate approximately equal to the maximal Lyapunov exponent. After 72 h, the log of mean error grows relatively slowly, departing from the linear evolution and entering a nonlinear phase with a steadily decreasing growth rate with increasing time. In this phase, the absolute intensity error started to deviate from the exponential growth. Finally, the curves of the log of mean errors in MCP and MSW reach the saturation level. Similarly, Kieu and Moon (2016) also reported that the forecast error of TC intensity in most of the operational numerical models grows rapidly at the initial stage, and the errors of TC intensity ultimately reach saturation after 72 h.

The log of mean error growth may be determined by a range of mechanisms in the different phases of error growth. In the initial stage in which the initial error grows linearly, the change of TC intensity may be greatly influenced by the initial conditions. However, at longer ranges the intensity and structure of a TC depend more on the large-scale environment than on the initial conditions (Kieu and Moon 2016). Previous studies have suggested that such a saturation of the TC intensity error appears to exist and may depend on specific environmental conditions, physical approximations, or the type of numerical model, such as an axisymmetric hurricane model or the Hurricane Weather Research and Forecasting (HWRF) Model (Yang et al. 2007; Hakim 2011, 2013).

The predictability of weather systems is limited by the chaotic nature of the atmosphere. The saturation theorem (Ding et al. 2010) implies that predictability is lost when the mean error reaches the saturation limit. In the present study, the predictability limits of the TC MCP and MSW are defined as the time at which the error reaches 95% of its saturation level, following Ding and Li (2007). As shown in Figs. 3a and 3b, the predictability limit obtained from the IBTrACS dataset for the TC MCP is ~102 h, which is comparable to (but slightly lower) than that of the TC MSW, which has a predictability limit of 108 h.

As shown above, the mean error growth and the predictability limits of TC intensity obtained by the NLLE approach are the average results of all TCs over the whole WNP basin. Considering that the TCs generated in different areas may have different characteristics (e.g., lifetime and intensity), we further use the NLLE method

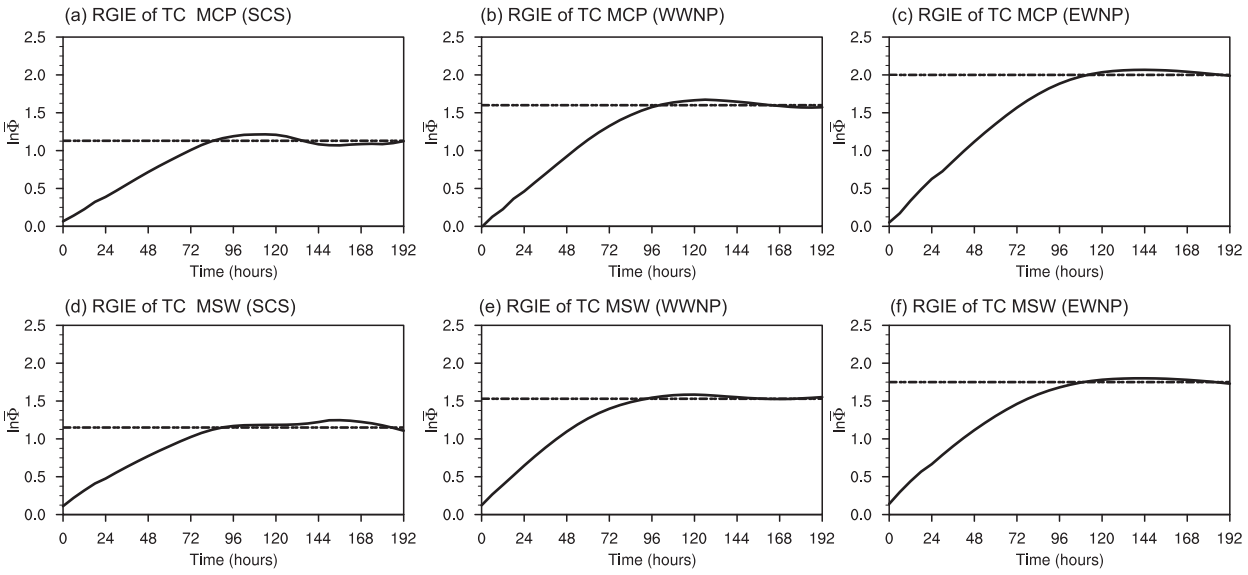

FIG. 7. As in Fig. 3, but for the mean error growth of the TC (a)–(c) minimum central pressure (MCP) and (d)–(f) maximum sustained wind (MSW) in the (a),(d) SCS; (b),(e) WWNP; and (c),(f) EWNP.

to quantitatively estimate the predictability limits of the MCP and MSW of the individual TC according to the 95% error saturation criterion. Figure 4 shows the probability distributions of the predictability limit of the TC MCP and MSW, which are sorted from lowest to highest. The modes of the predictability limit distribution for TC intensity are 72 h for both the TC MCP and MSW, with maximum probability values of 25.8% and 25.2%, respectively. The next highest frequencies occur at 96 h and then at 48 h.

Moreover, to obtain the spatial distributions of the predictability limits, the estimates of the predictability limit of the individual TC MCP and MSW based upon the TC genesis location are interpolated onto a 2° latitude by 2° longitude spatial grid across the whole WNP. Figures 5a and 6a show the spatial distributions of the predictability limits of the TC MCP and MSW over the whole WNP basin, respectively. The distributions of the predictability limits of the TC MCP and MSW are relatively consistent, with a pattern correlation coefficient of 0.8, which is significant at the 0.01 level. In addition, for both the TC MCP and MSW, the predictability limits range from 60 to 144 h over the WNP basin. There is a relatively high predictability limit of the TC MCP over the southeastern region of the WNP (>120 h), which is similar to the situation for the TC MSW. On the other hand, the predictability limit of the TC MCP is relatively low (84–108 h) in the west of the WNP (120.0°–140.0°E), and this is also similar to the distribution of the TC MSW. In addition, both the TC MCP and MSW have the lowest predictability limits (<72 h) in the SCS (110.0°–120.0°E). Overall, the meridional mean predictability limits of the TC MCP and MSW are also higher in the eastern WNP than in the SCS, and there is a gradual increase from 100°E to 180° in both cases (Figs. 5b and 6b).

As mentioned above, the distributions of the predictability limits of the TC MCP and MSW obtained by the NLLE method closely resemble the spatial pattern of the predictability limit of the TC tracks (corresponding to Fig. 5 in Z18), which ranges from 48 to 120 h, and depends largely on TC genesis location over the WNP basin. The pattern correlation coefficients between the distributions of the predictability limits of the TC tracks are 0.67 and 0.70 for the TC MCP and TC MSW, respectively, which are significant at the 0.01 level. Both meridional means of the predictability limits of the TC MCP and MSW obtained by the NLLE method are also similar to those of the TC tracks shown by Z18, who report that the predictability limit of the TC tracks shows a gradual increase from 100°E to 180°, as highlighted by the meridional mean. These results essentially indicate that the TC track is closely related to the TC intensity.

The above analysis reveals that the distributions of the predictability limits of the TC MCP and MSW depend largely on TC genesis location. One distinct feature in Figs. 5a and 6a is that the predictability limits of the TC MCP and MSW are generally lower in the SCS than east of 120°E over the WNP, so the SCS can be considered a separate region, based on the distribution of genesis location in Fig. 1. In addition, we divide the area east of 120°E over the WNP into two subregions (referred to as the WWNP and EWNP), using as the boundary the

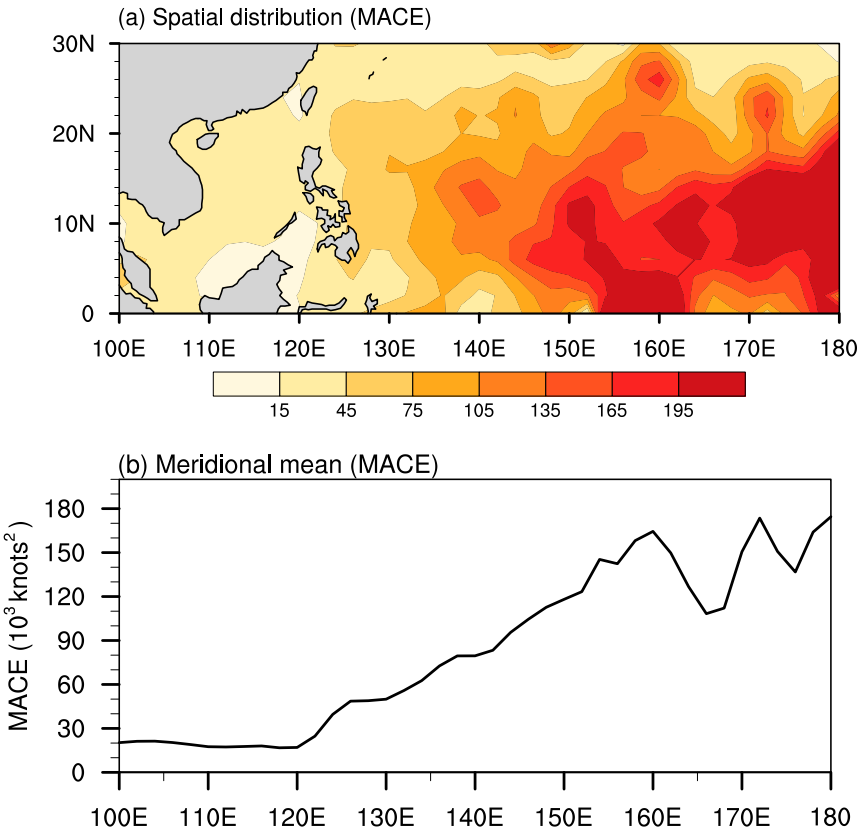

FIG. 8. (a) Spatial distribution of the TC modified accumulated cyclone energy (MACE; 10^3 kt^2) and (b) its meridional mean profile. Note that the spatial interpolations are based on the TC genesis location.

longitude (141°E) of the mean genesis location of all TCs over the whole WNP basin.

Figures 7a–c show the log of mean error of the TC MCP in the SCS, WWNP, and EWNP regions, respectively. The time taken for the log of mean error of the TC MCP to reach the saturation state gradually increases from the SCS to EWNP. This corresponds to the predictability limit of the TC MCP, with values of around 84, 96, and 120 h in the SCS, WWNP, and EWNP regions, respectively. Similarly, the log of mean error growth of the TC MSW in the SCS is the fastest to reach saturation state, followed by the WWNP and then the EWNP (Figs. 7d–f). The predictability limits of the TC MSW are about 84, 96, and 108 h in the SCS, WWNP, and EWNP, respectively. Clearly, there are no obvious differences in the predictability limits of the TC MCP and MSW in the SCS and the WWNP. However, in the EWNP, the predictability limit of the TC MCP is comparable to (but slightly higher than) that of the TC MSW. In both cases, the predictability limits of the TC MCP and MSW in the EWNP are much higher than those in the SCS, which is consistent with the characteristics of the spatial patterns shown in Figs. 5a and 6a. Moreover, it is also found that the saturation level of the log of mean errors in the WNP is much higher than in the SCS, and the errors get larger and larger from the SCS to EWNP (Figs. 7a–f). This is probably related to stronger TCs that form in the EWNP, which tend to be associated with larger errors in their evolution [e.g., rapid intensification (RI)] (Tao and Zhang 2015; Judt and Chen 2016). The TCs that form in the SCS appear to have a smaller error growth rate than TCs farther east, but their error saturation occurs at a much lower level, which yields a relatively short predictability limit. Additionally, as pointed out by Judt et al. (2016), the error of MSW for weaker and shorter-lived TCs likely saturates at lower values, because there is less energy at wavenumber 0 in those storms.

b. *Relationship between the predictability of TC intensity and the modified accumulated cyclone energy*

The accumulated cyclone energy (ACE) defined by Bell et al. (2000) has been increasingly used to measure TC activity. The annual ACE value gives a measure not

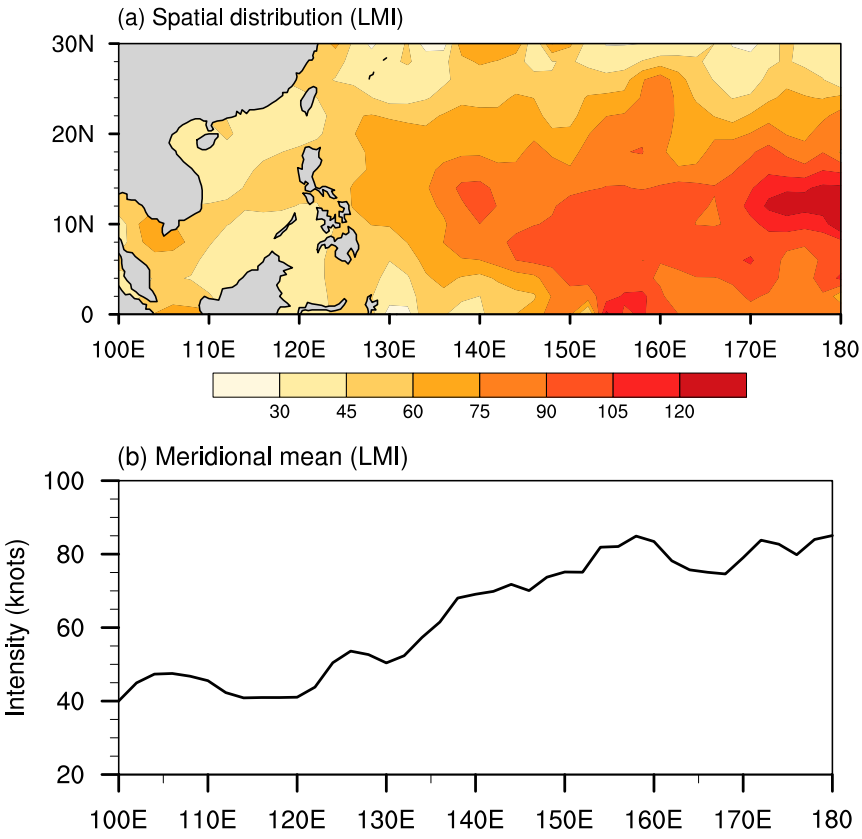

FIG. 9. As in Fig. 8, but for the lifetime maximum intensity (LMI, kt) and (b) its meridional mean profile.

only of the annual number of TCs, but also their lifetimes and intensities. The annual ACE is defined as the sum of the squares of the estimated 6-hourly MSW (in kt) for all the TCs with intensities of at least 35 kt. To illustrate why the distributions of the predictability limits of the TC MCP and MSW depend largely on TC genesis location, we define the modified accumulated cyclone energy (MACE) to describe the individual character of a TC's intensity. Our definition of MACE is similar to that in Camargo et al. (2005). In contrast to the value of annual ACE, the MACE for each TC is calculated as the sum of the squares of the particular TC's MSW for all times in which the TC intensity is at least 35 kt and so is independent of the annual number of TCs in the WNP. The MACE is based on the mean lifetime of the TC and the MACE equivalent wind speed, which is both a physically and statistically reasonable metric of individual TC activity.

Figure 8a shows the spatial distribution of the TC MACE calculated at the genesis locations. Similar to Fig. 5a, the MACE values of the TCs are interpolated onto a 2° latitude by 2° longitude spatial grid across the whole WNP basin. The spatial pattern of the MACE reflects the main characteristics of the distributions of the predictability limit for both the TC MCP and MSW. The spatial distribution of the TC MACE is significantly correlated with the distribution of the predictability limits of the TC MSW ($r = 0.75$, significant at the 0.01 level) and with the predictability limits of the TC MCP ($r = 0.73$, significant at the 0.01 level). There is relatively low MACE in the SCS, while high MACE is present over the southeastern region of the WNP, with two centers in this region. This result indicates that the predictability limit of the TC intensities may be associated with the TC MACE in the WNP basin.

The TC MACE contains information on both the lifetime of the TC and its wind speed, and the nature of TC activity depends on various characteristics of these components. Therefore, we next analyze separately the distributions of these components to study the possible changes in TC activity over the WNP basin. In the best track data, TC lifetimes depend on the definition of the first and last records of a TC, and the TC intensity is its lifetime maximum intensity (LMI). Figures 9a and 10a present the distributions of the lifetime and LMI for the TCs over the whole WNP basin, respectively.

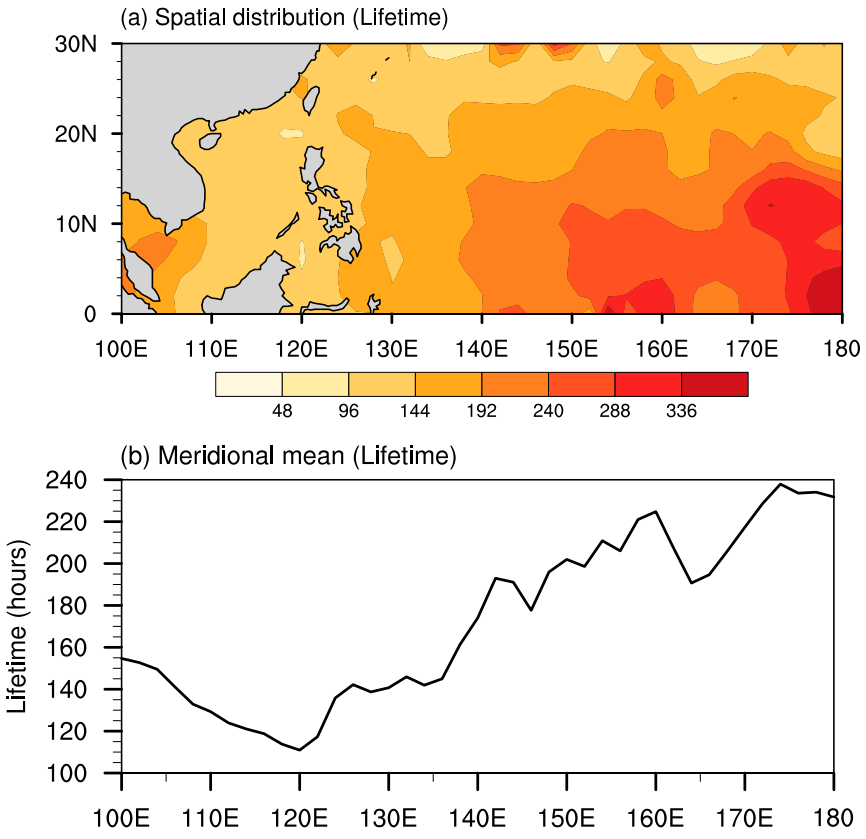

FIG. 10. As in Fig. 8, but for the TC lifetime (h) and (b) its meridional mean profile.

The lifetime of a TC ranges from ~96 to 288 h, and the LMI of the TC is between 30 and 120 kt. The spatial distribution of the TC lifetime is similar to that of the TC LMI, and these spatial distributions are consistent with the distribution of TC MACE shown in Fig. 8a. We also calculated the pattern correlations between the distributions of MACE, LMI, and lifetime over the WNP basin (Table 1). The MACE exhibits a pattern correlation with LMI and lifetime at 0.91 and 0.85, respectively (both significant at the 0.01 level), indicating that both of the LMI and lifetime of TC are very relevant to the MACE of TC. Moreover, the spatial distributions of TC lifetime and LMI appear to depend on the genesis locations of the TCs, which have a similar distribution to that of the TC MACE in Fig. 8a. This result indicates that the spatial distributions of the predictability limits of the TC MCP and MSW are related to those of the TC lifetime and LMI. Relatively long lifetime and relatively strong TCs are generated in the southeastern region of the WNP, corresponding to high TC MACE and high predictability of TC intensity. The predictability limits of the TC MCP and MSW appear to be lower in the SCS and the western WNP, which also corresponds well to relatively low MACE, relatively short lifetime, and relatively weak intensity of the TCs there. These results support our interpretation of the distribution of the predictability limits of TC intensity. It is likely that the predictability limits of TC intensity are generally associated with changes in TC lifetime and LMI and that a TC with a relatively long lifetime and relatively large LMI may favor relatively high predictability of TC intensity.

To know if uncertainty of land interaction causes changes in the predictability of TC intensity, we further calculate the predictability limit of intensity after removing data after landfall. As shown in Fig. 11, the predictability limits of MCP and MSW with landfall data exhibit pattern correlation with those of TC MCP and

TABLE 1. Pattern correlations between the modified accumulated cyclone energy (MACE), the lifetime maximum intensity (LMI), and the lifetime of TCs over the WNP basin based on observational data.

	MACE	LMI	Lifetime
MACE	1	—	—
LMI	0.91	1	—
Lifetime	0.85	0.84	1

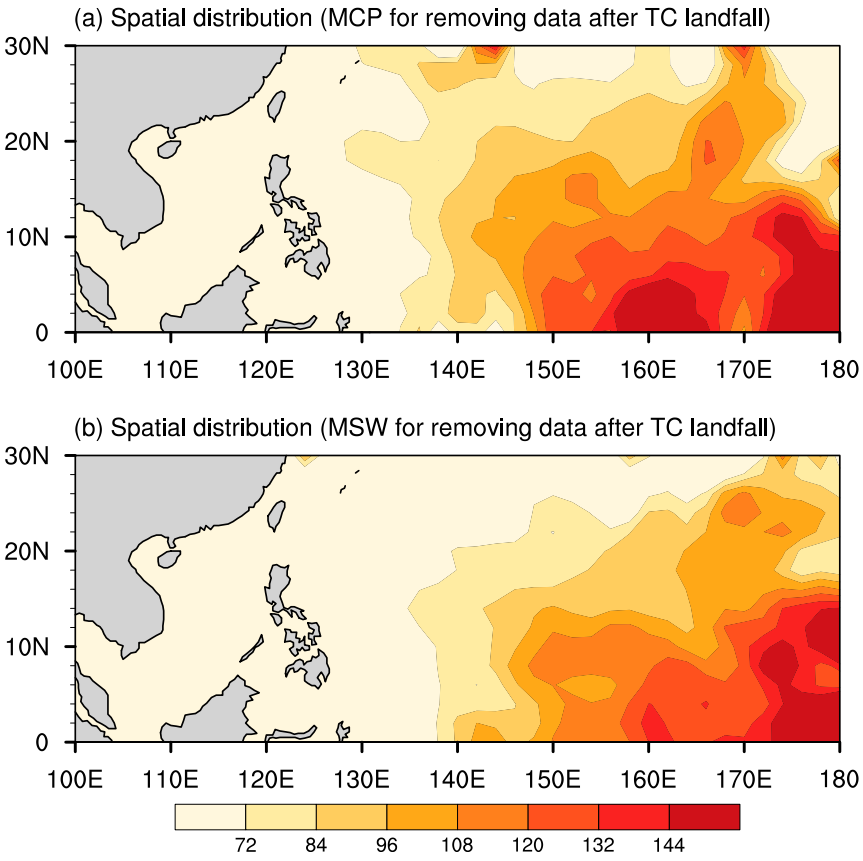

FIG. 11. As in Fig. 5a, but for the predictability limits of TC (a) MCP and (b) MSW with TC landfall data removed.

MSW without landfall data at 0.74 and 0.85, respectively (both significant at the 0.01 level). In addition, the pattern correlation coefficients are 0.90 and 0.94 between the predictability limits of the TC MCP and MSW with landfall data and their TC lifetime, which are significant at the 0.01 level. However, the pattern correlation coefficients are 0.77 and 0.83, respectively (both significant at the 0.01 level), if we do not consider the TC landfall (without landfall data). These results still indicate that the TC lifetime is well correlated with the predictability of TC intensity. Meanwhile, the uncertainty of TC landfall also has an effect on the TC intensity predictability and is somewhat determining the zonal distribution of the predictability, albeit the effect of land interaction is relatively small.

The emphasis on the TC genesis location or the LMI does not take into account the change in predictability limit through the TC life cycle. Therefore, we further examine how the predictability limits of intensity evolve as a function of the time that has evolved since the TC began. Here, the similarity criterion of finding a TC analog is based on the similarity of location and intensity at the time 24, 48, 72, and 96 h after TC genesis, respectively (and is not based on the similarity of the initial location and intensity at the genesis time). If the analogous TCs are found, the TC intensities predictability are computed using the same procedure that is given in appendix B, where the initial intensity error is the absolute difference of TC intensity at the time 24, 48, 72, and 96 h after TC genesis, respectively.

Figure 12 shows estimates of the predictability limit of the TC MCP and MSW as a function of the time that has evolved since the TC formed. The predictability limit of the TC MSW gradually decreases from 108 h at genesis time to 84 h four days after TC formation. However, for the TC MCP, the predictability limit shows more pronounced decrease from 102 h at the genesis time to 54 h four days after TC formation. These results indicate that the predictability limits of the TC MCP and MSW appear to evolve in the TC life cycle, and the TC intensities become less predictable as they evolve since the TC formed, consistent with the zonal gradient of TC intensity predictability shown in Figs. 5a and 6a.

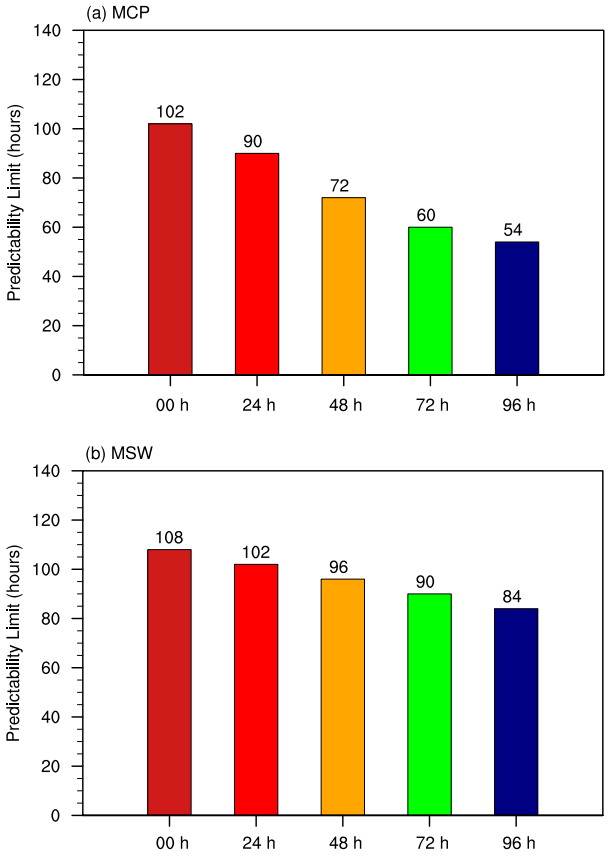

FIG. 12. Estimated predictability limit of TC (a) MCP and (b) MSW as a function of the time that has evolved since the TC formed.

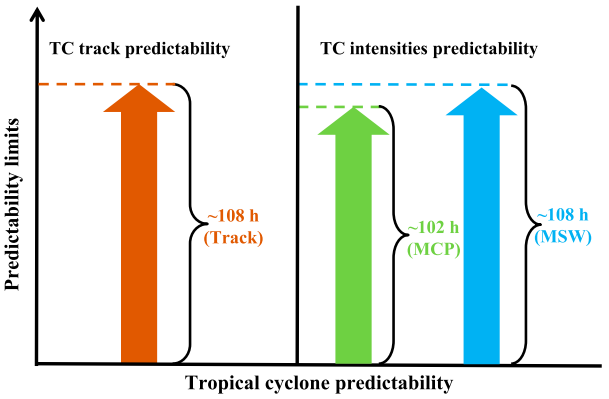

FIG. 13. Simplified diagram showing the range of estimates of TC track and intensity predictability obtained by the NLLE approach.

4. Summary and discussion

In this work, the predictability limits of the TC MCP and MSW over the western North Pacific (WNP) are investigated with the observed TC best track data using the NLLE method, which has been proposed to evaluate atmospheric and oceanic predictability. The predictability limit of the TC MCP obtained from the IBTrACS dataset is ~102 h, slightly lower than the predictability limit of TC MSW, which is ~108 h. Similar results were reported by Kieu and Moon (2016), who found that the predictability limit of TC intensity forecasts was 108–120 h in a low-order hurricane-scale dynamical model (Kieu and Moon 2016), thereby exceeding the performance of most numerical and statistical prediction models. Figure 13 summarizes the range of TC track and intensity predictabilities obtained by the NLLE approach. The predictability limits of the TC intensities are comparable to those of the TC tracks. These results provide a new perspective that enhances our understanding of the predictability limits of TCs, and is encouraging for TC prediction.

As these values of the limits (~102 and ~108 h) are general estimates of the predictability limits of the TC MCP and MSW over the whole WNP basin, and TC characteristics such as lifetime and the LMI vary widely with genesis location, we further examined the spatial distributions of the predictability limits of the TC MCP and MSW. The predictability limits of both TC MCP and MSW are relatively high in the southeastern WNP, exceeding 120 h at most locations. In contrast, the limits are relatively low in the SCS, less than 72 h. The spatial distribution of the predictability limit appears to depend on the TC genesis location. In addition, the distributions of the predictability limits of TC MCP and MSW are consistent with those of TC MACE, lifetime, and intensity (LMI). The regions where the TC intensity is relatively strong and the TC has a relatively long lifetime favor relatively high predictability of TC MCP and MSW.

Moreover, we used the NLLE approach to perform a quantitative analysis of how the predictability limits of intensity evolve as a function of the time that has evolved since the TC began. The predictability limit of TC MSW at the genesis location (108 h) gradually drops below the limit of 84 h at time 96 h after the TC formed, while the predictability limit of the TC MCP with a value of 102 h rapidly falls to 54 h. This result reveals an evolving predictability limit of TC intensity throughout the TC life cycle, and these reduced limits may be associated with the remaining lifetime of the TCs.

There are several limitations to the present study. First, because of the use of best track data to find the analogous TCs and calculate the mean error growth, it is still likely that the predictability limits of the TC MCP and MSW are underestimated. Given the relatively short observational records of TC best track data, some false analogs are inevitably in the best track data, which means that initial errors of TC intensities can be quite large (because it is be more difficult to identify analogous TCs). Meanwhile,

because of the sparse observations before the 1970s when aircraft and satellite were not available, the IBTrACS dataset may include some estimated uncertainty of the TC intensity, thereby possibly introducing uncertainty in estimating the predictability limit over the whole WNP basin. Consequently, our estimate of the predictability limit of the TC tracks will inevitably include uncertainties. Therefore, the predictability of TC intensities should be assessed further with a longer period of observed TC best track data or a series of idealized simulations using a more realistic numerical model. Second, the observed TC best track data do not contain information on large-scale environmental variables and the internal TC processes, so the NLLE method could not be used to explore the impact of these factors on TC intensity predictability based on the best track data. Although the land effect is removed through removing the landfall data, we cannot remove land effect like in modeling studies in which the land can be "truly" removed by artificially change the surface parameters. Further work will be necessary to examine their influence on the predictability of TC intensity in different TC cases using a more realistic model.

Acknowledgments. We thank three anonymous reviewers for helpful comments and suggestions. This research was jointly supported by the National Natural Science Foundation of China for Excellent Young Scholars (41522502), the National Program on Global Change and Air-Sea Interaction (GASI-IPOVAI-03, GASI-IPOVAI-06), and the National Key Technology Research and Development Program of the Ministry of Science and Technology of China (2015BAC03B07).

APPENDIX A

An Algorithm for Finding Two Analogous TCs

Let the TC $\{x_i[\theta_i(t_k), \varphi_i(t_k)], \quad k = 0, 1, 2, \ldots, m-1, i = 1, 2, \ldots, N\}$ be a set of points of TC position, where m represents the length of a TC time series, N represents the total number of TCs, and $\theta_i(t_k)$ and $\varphi_i(t_k)$ represent the longitude and latitude, respectively. With continuous TC position data, the distance (along a great circle) between two independent TCs is given by

$$d_{ij}(t_k) = R \times \arccos\{\sin\varphi_i(t_k)\sin\varphi_j(t_k) + \cos\varphi_i(t_k)\cos\varphi_j(t_k)[\theta_i(t_k) - \theta_j(t_k)]\}, \quad \text{(A1)}$$

where R is the average radius of Earth and t_k are the times corresponding to TC_i and TC_j.

The determination of two analogous TCs is based on the initial distance $d_{1j}(t_0)$ and the evolutionary distance d_e. The algorithm used to find two analogous TCs from all TCs over the WNP basin is briefly described as follows.

- Step 1. Taking TC_1 as the reference TC, with genesis location $x_1[\theta_1(t_0), \varphi_1(t_0)]$ defined as the reference initial position at the initial time (genesis time) t_0, we first seek the genesis location $x_j[\theta_j(t_0), \varphi_j(t_0)]$ of TC_j. The initial distance $d_{1j}(t_0)$ is the distance between the genesis locations of TC_1 and TC_j. To ensure similarity of the large-scale environmental steering flow for the two TCs, TC_j should be formed in a similar "season" but in a different year to TC_1 (i.e., ±45 days from the genesis time of the reference TC), and the differences in initial intensities between the TC_1 and TC_j should be small.
- Step 2. Within a short initial period, the evolutionary distance d_e is used to measure the degree of similarity of the tracks of TC_1 and TC_j. Note that in a previous study the choice of the initial evolutionary stage depended on the persistence of the variable of interest (Li and Ding 2011). In the present study, because it is impossible to obtain the persistence of the TC tracks, we set the initial evolutionary stage as two 6-h time steps (i.e., 12 h), and found that the predictability results of the TC tracks are not sensitive to the choice of this parameter. Within the initial evolutionary stage, the evolutionary distance d_e between the TC_1 $x_1[\theta_1(t_k), \varphi_1(t_k)]$ and TC_j $x_j[\theta_j(t_k), \varphi_j(t_k)]$ is given by

$$d_e = \sqrt{\frac{1}{K+1}\sum_{k=0}^{K}[d_{1j}(t_k)]^2}, \quad K = 2, \quad \text{(A2)}$$

  where K is the steps of the initial evolutionary interval, and $d_{1j}(t_k)$ is the initial separation between TC_1 $x_1[\theta_1(t_k), \varphi_1(t_k)]$ and TC_j $x_j[\theta_j(t_k), \varphi_j(t_k)]$.
- Step 3. The total distance d_t, taking into account not only the initial distance but also the evolutionary distance, is found by adding $d_{1j}(t_0)$ and d_e:

$$d_t = d_{1j}(t_0) + d_e. \quad \text{(A3)}$$

  If d_t is small, it is likely that the TC_1 $x_1[\theta_1(t_k), \varphi_1(t_k)]$ and TC_j $x_j[\theta_j(t_k), \varphi_j(t_k)]$ are analogous TCs at the initial time. The constraint of the total distance d_t has two components: the initial distance and evolutionary distance. Such a constraint condition allows us to exclude a large portion of all nonanalogous TCs, and thereby find the analogous TC_j for the reference TC_1 over the WNP basin.

APPENDIX B

An Algorithm for Estimating NLLE and RGIE from the Best Track Data

For every TC_i, the value of total distance d_t can be determined using the algorithm in appendix A. The analogous

TC_j of the reference TC_i is only chosen from all TCs over the whole WNP basin if the total distance d_t is small. Let the TC $[y_i(t_k), k = 0, 1, 2, \ldots, M-1, i = 1, 2, \ldots, N]$ be a set of TC intensities at 6-hourly intervals, where M represents the length of a TC time series, N represents the total number of TC, and $y_i(t_k)$ is the intensity at each time.

- Step 1. The initial intensity error is the absolute difference in TC intensity between the reference TC_i $[y_i(t_k), k = 0, 1, 2, 3, \ldots, m-1]$ and its analogous TC_j at genesis time, which can be denoted as follows:

$$I_i(t_0) = y_i(t_0) - y_j(t_0). \tag{B1}$$

- Step 2. At time $t_k = k \times \Delta$ $(k = 1, 2, \ldots, M)$, the M is the total number of TC intensity points, and the symbol Δ represents the time interval which is 6 h in the present study. The reference TC_i will have moved from $y_i(t_0)$ to $y_i(t_k)$, and its analogous TC_j will have moved from $y_j(t_0)$ to $y_j(t_k)$ (see Fig. 2b). The initial difference $I_i(t_0)$ then becomes the difference $I_i(t_k)$, which is given by

$$I_i(t_k) = y_i(t_k) - y_j(t_k). \tag{B2}$$

To estimate the NLLE, it is necessary to examine the growth rate of the initial intensity error between two initially close TCs over the whole WNP basin. The growth rate of the initial error (absolute difference in TC initial intensity) during the evolutionary interval (t_k) is

$$\xi_i(t_k) = \frac{1}{t_k} \ln \frac{I_i(t_k)}{I_i(t_0)}, \quad (k = 1, 2, 3, \ldots, M), \tag{B3}$$

where $I_i(t_0)$ is the initial error in intensity between the reference TC_i and its analogous TC_j, and the difference $I_i(t_k)$ is the initial intensity error $I_i(t_0)$ at time t_k. With k gradually increasing, we can obtain the variation in $\xi_i(t_k)$ as a function of the evolution time t_k $(k = 1, 2, 3, \ldots, M)$.

- Step 3. Steps 1 and 2 are repeated for every TC, and the growth rates of intensity error for each reference TC $\{[y_1(t_k), y_2(t_k), \ldots, y_i(t_k)], (i = 1, 2, 3, \ldots, N)\}$ are given by

$$\xi_i(t_k) = \frac{1}{t_k} \ln \frac{I_i(t_k)}{I_i(t_0)}, \quad (i = 1, 2, 3, \ldots, N; \; k = 1, 2, 3, \ldots, M), \tag{B4}$$

where $i = N$ is the total number of all TCs over the whole WNP basin, the evolution time from the initial time t_0 is $t_k = k \times \Delta$ $(k = 1, 2, 3, \ldots, M)$, $I_i(t_0)$ is the initial error of intensity between the reference TC and its analogous TC, and the difference $I_i(t_k)$ is the initial intensity error $I_i(t_0)$ at time $t_k I_i(t_k)$ is the evolution of $I_i(t_0)$ with evolution time t_k. It follows that the mean growth rates of the initial intensity error for all reference TCs is given by

$$\overline{\xi}(t_k) = \frac{1}{N} \sum_{i=1}^{N} \xi_i(t_k) = \frac{1}{N} \sum_{i=1}^{N} \left[\frac{1}{t_k} \ln \frac{I_i(t_k)}{I_i(t_0)} \right] = \frac{1}{t_k} \ln \left[\sqrt[N]{\frac{I_1(t_k)}{I_1(t_0)} \frac{I_2(t_k)}{I_2(t_0)} \cdots \frac{I_N(t_k)}{I_N(t_0)}} \right]. \tag{B5}$$

- Step 4. The mean relative growth of initial error (RGIE) for all reference TCs is given by

$$\overline{\Phi}(t_k) = \exp[\overline{\xi}(t_k) t_k] = \sqrt[N]{\frac{I_1(t_k)}{I_1(t_0)} \frac{I_2(t_k)}{I_2(t_0)} \cdots \frac{I_N(t_k)}{I_N(t_0)}}, \quad (k = 1, 2, 3, \ldots, M). \tag{B6}$$

Note that the description of the algorithm for estimating NLLE and RGIE from the best track data is derived from that in Li and Ding (2011) and Ding et al. (2016) with some slight modifications. In this work, the time at which the mean error reaches 95% of the saturation level can also be defined as the mean predictability limit of all TC intensities (Ding et al. 2011; Li and Ding 2013).

REFERENCES

Bell, G. D., and Coauthors, 2000: Climate assessment for 1999. *Bull. Amer. Meteor. Soc.*, **81**, S1–S50, https://doi.org/10.1175/1520-0477(2000)81[s1:CAF]2.0.CO;2.

Brown, B. R., and G. J. Hakim, 2013: Variability and predictability of a three-dimensional hurricane in statistical equilibrium. *J. Atmos. Sci.*, **70**, 1806–1820, https://doi.org/10.1175/JAS-D-12-0112.1.

Camargo, S. J., A. G. Barnston, and S. E. Zebiak, 2005: A statistical assessment of tropical cyclone activity in atmospheric general circulation models. *Tellus*, **57A**, 589–604, https://doi.org/10.3402/tellusa.v57i4.14705.

Chen, B. H., J. P. Li, and R. Q. Ding, 2006: Nonlinear local Lyapunov exponent and atmospheric predictability research. *Sci. China*, **49D**, 1111–1120, https://doi.org/10.1007/s11430-006-1111-0.

DeMaria, M., C. R. Sampson, J. A. Knaff, and K. D. Musgrave, 2014: Is tropical cyclone intensity guidance improving? *Bull. Amer. Meteor. Soc.*, **95**, 387–398, https://doi.org/10.1175/BAMS-D-12-00240.1.

Ding, R. Q., and J. P. Li, 2007: Nonlinear finite-time Lyapunov exponent and predictability. *Phys. Lett.*, **364A**, 396–400, https://doi.org/10.1016/j.physleta.2006.11.094.

——, G. L. Feng, S. D. Liu, S. K. Liu, S. X. Huang, and Z. T. Fu, 2007: Nonlinear atmospheric and climate dynamics in China (2003-2006): A review. *Adv. Atmos. Sci.*, **24**, 1077–1085, https://doi.org/10.1007/s00376-007-1077-7.

——, J. P. Li, and K. H. Seo, 2010: Predictability of the Madden–Julian oscillation estimated using observational

data. *Mon. Wea. Rev.*, **138**, 1004–1013, https://doi.org/10.1175/2009MWR3082.1.

——, ——, and ——, 2011: Estimate of the predictability of boreal summer and winter intraseasonal oscillations from observations. *Mon. Wea. Rev.*, **139**, 2421–2438, https://doi.org/10.1175/2011MWR3571.1.

——, ——, F. Zheng, J. Feng, and D. Q. Liu, 2016: Estimating the limit of decadal-scale climate predictability using observational data. *Climate Dyn.*, **46**, 1563–1580, https://doi.org/10.1007/s00382-015-2662-6.

Elsberry, R. L., T. D. Lambert, and M. A. Boothe, 2007: Accuracy of Atlantic and eastern North Pacific tropical cyclone intensity forecast guidance. *Wea. Forecasting*, **22**, 747–762, https://doi.org/10.1175/WAF1015.1.

Emanuel, K., and F. Q. Zhang, 2016: On the predictability and error sources of tropical cyclone intensity forecasts. *J. Atmos. Sci.*, **73**, 3739–3747, https://doi.org/10.1175/JAS-D-16-0100.1.

Gopalakrishnan, S. G., F. Marks Jr., X. Zhang, J.-W. Bao, K.-S. Yeh, and R. Atlas, 2011: The experimental HWRF system: A study on the influence of horizontal resolution on the structure and intensity changes in tropical cyclones using an idealized framework. *Mon. Wea. Rev.*, **139**, 1762–1784, https://doi.org/10.1175/2010MWR3535.1.

Hakim, G. J., 2011: The mean state of axisymmetric hurricanes in statistical equilibrium. *J. Atmos. Sci.*, **68**, 1364–1376, https://doi.org/10.1175/2010JAS3644.1.

——, 2013: The variability and predictability of axisymmetric hurricanes in statistical equilibrium. *J. Atmos. Sci.*, **70**, 993–1005, https://doi.org/10.1175/JAS-D-12-0188.1.

Judt, F., and S. S. Chen, 2016: Predictability and dynamics of tropical cyclone rapid intensification deduced from high-resolution stochastic ensembles. *Mon. Wea. Rev.*, **144**, 4395–4420, https://doi.org/10.1175/MWR-D-15-0413.1.

——, ——, and J. Berner, 2016: Predictability of tropical cyclone intensity: Scale-dependent forecast error growth in high-resolution stochastic kinetic-energy backscatter ensembles. *Quart. J. Roy. Meteor. Soc.*, **142**, 43–57, https://doi.org/10.1002/qj.2626.

Kaplan, J., and Coauthors, 2015: Evaluating environmental impacts on tropical cyclone rapid intensification predictability utilizing statistical models. *Wea. Forecasting*, **30**, 1374–1396, https://doi.org/10.1175/WAF-D-15-0032.1.

Kieu, C. Q., and Z. Moon, 2016: Hurricane intensity predictability. *Bull. Amer. Meteor. Soc.*, **97**, 1847–1857, https://doi.org/10.1175/BAMS-D-15-00168.1.

Knapp, K. R., and M. C. Kruk, 2010: Quantifying interagency differences in tropical cyclone best-track wind speed estimates. *Mon. Wea. Rev.*, **138**, 1459–1473, https://doi.org/10.1175/2009MWR3123.1.

——, ——, D. H. Levinson, H. J. Diamond, and C. J. Neumann, 2010: The International Best Track Archive for Climate Stewardship (IBTrACS) unifying tropical cyclone data. *Bull. Amer. Meteor. Soc.*, **91**, 363–376, https://doi.org/10.1175/2009BAMS2755.1.

Landsea, C. W., and J. L. Franklin, 2013: Atlantic hurricane database uncertainty and presentation of a new database format. *Mon. Wea. Rev.*, **141**, 3576–3592, https://doi.org/10.1175/MWR-D-12-00254.1.

Li, J. P., and R. Q. Ding, 2011: Temporal–spatial distribution of atmospheric predictability limit by local dynamical analogs. *Mon. Wea. Rev.*, **139**, 3265–3283, https://doi.org/10.1175/MWR-D-10-05020.1.

——, and ——, 2013: Temporal–spatial distribution of the predictability limit of monthly sea surface temperature in the global oceans. *Int. J. Climatol.*, **33**, 1936–1947, https://doi.org/10.1002/joc.3562.

Liu, J., W. Li, L. Chen, J. Zuo, and P. Zhang, 2016: Estimation of the monthly precipitation predictability limit in China using the nonlinear local Lyapunov exponent. *J. Meteor. Res.*, **30**, 93–102, https://doi.org/10.1007/s13351-015-5049-z.

Lorenz, E. N., 1963: Deterministic nonperiodic flow. *J. Atmos. Sci.*, **20**, 130–141, https://doi.org/10.1175/1520-0469(1963)020<0130:DNF>2.0.CO;2.

——, 1969: Atmospheric predictability as revealed by naturally occurring analogues. *J. Atmos. Sci.*, **26**, 636, https://doi.org/10.1175/1520-0469(1969)26<636:APARBN>2.0.CO;2.

Palmer, T., A. Döring, and G. Seregin, 2014: The real butterfly effect. *Nonlinearity*, **27**, R123, https://doi.org/10.1088/0951-7715/27/9/R123.

Ruf, C. S., and Coauthors, 2016: New ocean winds satellite mission to probe hurricanes and tropical convection. *Bull. Amer. Meteor. Soc.*, **97**, 385–395, https://doi.org/10.1175/BAMS-D-14-00218.1.

Tao, D., and F. Zhang, 2014: Effect of environmental shear, sea-surface temperature, and ambient moisture on the formation and predictability of tropical cyclones: An ensemble-mean perspective. *J. Adv. Model. Earth Syst.*, **6**, 384–404, https://doi.org/10.1002/2014MS000314.

——, and ——, 2015: Effects of vertical wind shear on the predictability of tropical cyclones: Practical versus intrinsic limit. *J. Adv. Model. Earth Syst.*, **7**, 1534–1553, https://doi.org/10.1002/2015MS000474.

Weng, Y., and F. Zhang, 2016: Advances in convection-permitting tropical cyclone analysis and prediction through EnKF assimilation of reconnaissance aircraft observations. *J. Meteor. Soc. Japan*, **94**, 345–358, https://doi.org/10.2151/jmsj.2016-018.

Yang, B., Y. Wang, and B. Wang, 2007: The effect of internally generated inner-core asymmetries on tropical cyclone potential intensity. *J. Atmos. Sci.*, **64**, 1165–1188, https://doi.org/10.1175/JAS3971.1.

Zhang, F., and D. D. Tao, 2013: Effects of vertical wind shear on the predictability of tropical cyclones. *J. Atmos. Sci.*, **70**, 975–983, https://doi.org/10.1175/JAS-D-12-0133.1.

——, and Y. Weng, 2015: Predicting hurricane intensity and associated hazards: A five-year real-time forecast experiment with assimilation of airborne Doppler radar observations. *Bull. Amer. Meteor. Soc.*, **96**, 25–33, https://doi.org/10.1175/BAMS-D-13-00231.1.

Zhang, Y., Z. Meng, F. Zhang, and Y. Weng, 2014: Predictability of tropical cyclone intensity evaluated through 5-yr forecasts with a convection-permitting regional-scale model in the Atlantic basin. *Wea. Forecasting*, **29**, 1003–1023, https://doi.org/10.1175/WAF-D-13-00085.1.

Zhong, Q., L. Zhang, J. Li, R. Ding, and J. Feng, 2018: Estimating the predictability limit of tropical cyclone tracks over the western North Pacific using observational data. *Adv. Atmos. Sci.*, in press, https://doi.org/10.1007/s00376-018-8008-7.

Zhu, L., and Coauthors, 2016: Prediction and predictability of high-impact western Pacific landfalling Tropical Cyclone Vicente (2012) through convection-permitting ensemble assimilation of Doppler radar velocity. *Mon. Wea. Rev.*, **144**, 21–43, https://doi.org/10.1175/MWR-D-14-00403.1.